Research Article

Lawend Kamal Askar*, Suhaib Yahya Kasim Al-Darzi, and Bayar Jafar Mohamed Al-Sulayfani

Experimental and numerical investigation on composite beam–column joint connection behavior using different types of connection schemes

https://doi.org/10.1515/eng-2024-0087
received May 28, 2024; accepted August 22, 2024

Abstract: Over the past few decades, composite joints have been regarded as one of the most promising approaches. After reviewing the research articles dealing with composite beam-column joints, it can be withdrawn that few researchers studied and developed different types of composite beam-column joints. The objectives of this paper to study the effect and behavior of different connection types on the composite beam – column joint under repeated loading as well as to investigate new forms of slab connection with column flange in composite connection joints, aiming to enhance the behaviors of the joints and make the slab endure a part of the load in a more efficient way. Five specimens with various connection types were tested to failure; the composite model number two (CM2) was considered the control specimen. Regarding the ultimate moment, the result found that CM5 has moment 50.47% more than control specimen, the lowest rotation value was in CM5. The general behaviours of the FEM were in good accordance with the experiment results. According to the parametric a higher yield strength is more rigid stiffer, the effect of web thickness on the load is too small and increase in load resistance with an increase in beam flange thickness.

*** Corresponding author: Lawend Kamal Askar,** Highways and Bridges Engineering, Technical College of Engineering, Duhok Polytechnic University (DPU) and University of Mosul, Duhok, Iraq,
e-mail: Lawend.Kamal@dpu.edu.krd
Suhaib Yahya Kasim Al-Darzi: Civil Engineering Department, College of Engineering, University of Mosul, Mosul, Iraq,
e-mail: suhaib.qasim@uomosul.edu.iq
Bayar Jafar Mohamed Al-Sulayfani: Civil Engineering Department, College of Engineering, University of Mosul, Mosul, Iraq,
e-mail: dr.bayar.alsulayvani@uomosul.edu.iq

Keywords: composite, connections, joints, repeated, special reinforced

1 Introduction

In the past, engineers had two distinct points of view and had to choose either concrete or steel constructions. More efficient solutions are now possible through composite constructions by carefully combining both elements. Optimized solutions regarding structural performance, structure weight, construction time, and costing procedure can be found. In composite frames, beam–column joints were the most critical components. Many studies have focused on the behavior of bare steel beam columns. They neglected the joint connection behavior and the steel detail's stiffness and moment capacity [1]. However, including more realistic joint effects requires comprehending the composite joint structure. A fundamental basis for the design has not been confirmed. In composite joint, the presence of variables in the existing database of test results only covers the subject in a patchy way [2]. The previous version of Eurocode 4 contained design guidelines for calculating and designing composite parts, including beams, columns, and slabs; the design of the composite joint parts was not detailed due to a lack of guidance in composite joint design [3]. The cooperation of the concrete parts was often ignored [4]. Recently, the study concentrated on the column and beam component capacities. However, the behavior of the composite joint is still not well realized [5]. In an experimental study, Xiao *et al.* [6] aimed to determine the variation in steel details of beam and column interaction with composite slab. The study focuses on moment and rotation in the joint. The failure mode other than the ductile yielding of rebars or compact steel sections limits the rotation capacity [7]. Liew *et al.* [8] worked on a composite structure (concrete-steel), slab consist of reinforced concrete and steel beam work as rigid

composite connections enhances the ability of deformation and the load capacity as compared with the use of steel connection only. Kuhlmann *et al.* [9] study defining the joint ductility in composite joint structures subjected to extreme loading. Malaska [10] found that the strength of concrete is unaffected by joint moment rotation. Demonceau and Jaspart [11] used two columns and the third column between them was centrally removable to test a two-dimension composite connection frame (concrete-steel). The test proved that ductile joints play a vital role in forming the catenary movement in beams. Large rotation capacity and strong resistance in the web cleat and flush endplate connection were demonstrated by the tests conducted in the tensile catenary range [12]. Sun *et al.* [13] used experimental and computational analysis to investigate the behavior of hollow structural section beam–column joint connections; the joint is considered as semi rigid. Welding steel components together creates a connection with a high level of stiffness and strength. If the weld is done correctly, a stiff connection can be formed; fasteners may be required, depending on the type of loading [14]. Wang *et al.* [15] suggested an alternate approach for internal diaphragms to achieve fabrication convenience. The beam flange is welded to the diaphragm, and the beam web is bolted to the column using the shear connection. Song *et al.* [16] revealed that flexural failure of the steel beam close to the panel zone was the primary cause of the joint failure by testing full-scale bolted joints. Zandonini *et al.* [17] focused on an experimental investigation for composite frames under the loss of column scenario; the test revealed the need for improved joint design and highlighted the main elements of the floor system; nonetheless, research on this topic is still restricted. The study includes concrete slab as well as beam–column joint. Firdaus *et al.* [18] suggested that the bottom flange of the beam pushes the flange of column in connection joint when rotation of connection becomes maximum. Furthermore, Local buckling caused by height compression was found at the column's flange. On the other hand, Gusset plates did not experience any failure modes. End plate connections are always welded to the flange and web of the beam and bolted to the column on site, the behavior of the end plate connection turns on the stiffness of the column flange near the connection [19]. Chen *et al.* [20] examined four beam column joints type and the thickness of the composites slab, bending moment, and axial force created at the joints were illustrations for structural responses, and typical failure conditions were demonstrated and explained. Skarmoutsos and Kuhlmann [21] dealt with beam column joints with endplate connectors consisting of steel specimens, and steel-concrete composite specimens with seismic behavior were examined in a series of experiments. However, research by Salah *et al.* [22] discovered that data about joint behavior are still lacking, and the connection shape has a major impact on the performance of the composite joint as well.

Numerical and analytical models for simulating composite beam–column joint behavior have been developed [7,23–28]. Several studies [29–32] used FE models to look into the structure under the case of column loss. However, Aminuddin *et al.* [5] investigated the beam-to-column connection behavior utilizing rectangular gusset plates with steel cold-formed sections. The goal was to see how the strength, stiffness, and flexibility of the connection were. A FE model was created using ABAQUS software for composite beam–column connection subjected to monotonic and symmetric hogging moments. Following that, an analysis was carried out to examine the elements that influence the behavior of composite joints; welded and bolted connections are the two options available for this application [33]. Kochem and Nardin [34] investigated the beam–column behavior of composite connection using a numerical model using the ABAQUS FE code. The results revealed that the increase in slab concrete strength had a minimal effect on the moment capacity. Mou *et al.* [35] conducted a numerical examination of reinforced concrete slabs with composite connection joints by testing the capabilities of flexure. The FE models were developed to represent the composite joint stress distribution [36]. A nonlinear numerical macro-modelling approach was proposed and validated by Fasan *et al.* [37] to anticipate and evaluate the steel–concrete composite joints. Various steel–concrete composite joint configurations can vary depending on the position of the joint, the type of connection (bolted or welded), and other factors. It is possible to construct the typical mechanisms in which the concrete slab itself contributes to the complicated performance.

Handhal *et al.* [1] presented the research, which examined how various steel sections might strengthen the beam–column joints. A theoretical study was conducted utilizing finite element analysis (FEA) to simulate beam–column connection laced with steel sections. In order to implement the parametric research, the concrete beam was reinforced in a variety of configurations using steel sections. The findings demonstrated that the steel section strengthening increased the joint's flexural strength, but these improvements were limited because of the concrete's strength limitation. Seismic upgradation of reinforced concrete beams enhanced using ferrocement laminates based on wasted catalyst and externally bonded is studied by Balamuralikrishnan *et al.* [38]. The purpose of the study is to compare under two-point loading conditions. The flexural, shear, and combined effect of the flexural and shear behavior of reinforced concrete

beams strengthened with externally bonded spent catalyst-based ferrocement laminates to the control beams (unstrengthened). The strength, yield load, ultimate load, stiffness, ductility, and associated failure modes of the flexural and shear performances of all tested beams were thus investigated. Rajić *et al.* [39] conducted possible analytical methods and a parametric FEA of cold-formed steel-concrete composite beams in bending. The examined beams consist of concrete slabs joined by demountable shear connections and cold-formed steel channels arranged back to back. A solid concrete slab atop a profiled metal sheet was analyzed. It is shown that concrete slab designs and beam bending capability are highly influenced by the steel channel's thickness and degree of shear connection. A comparison of the maximum bending capabilities found in FE studies shows high agreement with analytical methods.

The scope of the review is to gain further understanding of the composite connection joint behavior after reviewing the available research articles dealing with composite connection joints. By reviewing previous research, it was found that the composite connection joint capacity is an essential component of this review. Experimental research for joint connection details is vital in understanding joint strength's mechanisms, the composite joints are fully rigid joint or ideally pinned joint, the moment–rotation relationship joints of the structure applied to the semi-rigid joint connections and the increase in slab concrete strength had minimal effect on the moment capacity. It can be concluded from a review of the research articles that are currently available on the subject that although few researchers were able to study and develop various types of composite beam–column joints, there was also a lack in the study of composite beam–column joints when steel members were joined to reinforce concrete members. In order to improve joint behaviors and make the slab withstand a portion of the load more effectively, the goals of this study are to examine the impact and behavior of various connection types on the composite beam–column joint under repeated loading as well as to explore novel forms of slab connection with column flange in composite connection joints.

2 Experimental program

The test was designed to investigate the effect of joining the composite steel-concrete beam to the steel column. The effect of using different types of stiffening will be considered to understand their effect on the behavior of the beam. The main item considered in the experiment is the rotation of the beam with the types or stiffening methods adopted under repeated loads.

The study was carried out by adopting an experimental program that used a steel IPE 160 beam with a length of 1,000 mm and a steel HEA 200 column with a length equal to 2,000 mm. The steel end plate connects the beam to the column, is welded to the beam, and is fastened to the column with six bolts of 12 mm in diameter; the dimensions of a reinforced concrete slab is 1,000 mm × 500 mm with 100 mm thickness. Five shear studs were welded on the top flange of the beam. Figure 1 illustrates the cross-section of the steel I beam, a cross-section of the steel H column, and the end plate dimensions, respectively. Reinforcement steel bars with a diameter of 10 mm were employed for all model specimens in two directions with spacing 200 mm × 200 mm as shown in Figure 2.

Figure 3 shows the specimens being prepared before casting. Concrete work will be done within the laboratory, and concrete's compressive strength and flexure strength will be experimentally tested. The water-to-cement ratio

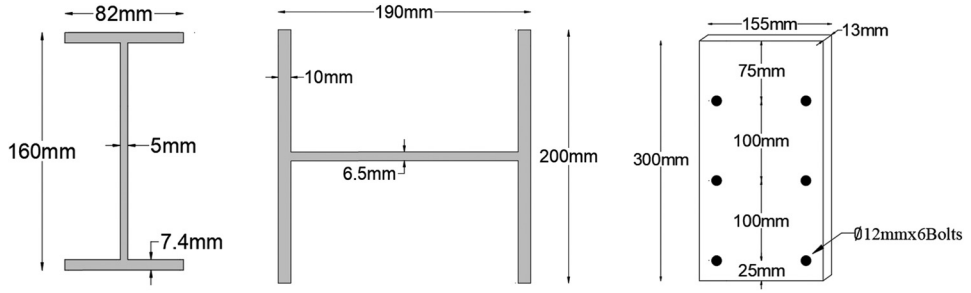

Figure 1: Cross sections of IPE 160 beam, HEA 200 A column, and end plate dimensions. (a) Cross section of IPE 160 beam. (b) Cross section of HEA 200 A column. (c) End plate dimensions.

Figure 2: Reinforcement of steel.

Figure 3: Preparing specimens for casting.

was 0.42, and the obtained mixing proportion was (cement: sand: gravel) 1:1.5:3; a slump of 80 mm was determined. Compressive strength results for 7 and 28 days were 19.03 and 24.86 MPa, respectively, and the average flexure strength of concrete was 6.03 MPa.

The description of the rig details is included in Table 1. A hydraulic jack will be employed to test specimens in the laboratory. The testing apparatus was set up to apply the load vertically, as illustrated in Figure 4. By using hydraulic

Table 1: Rig details description

Code in figure	Description
1	Steel lateral support for hydraulic jack
2	Hydraulic jack base
3	Hydraulic jack
4	Reinforced slab
5	HEA 200 column
6	IPE 160 beam
7	Loading steel pad

Figure 4: Testing rig details.

jacks installed on the test apparatus, repeated load will be applied to the specimen. The load will be applied at the free end of the composite beam, and the column will be fixed on both ends. This arrangement facilitated column specimens for accurate adjustment.

The load was measured through load cells positioned in the region between a seat and a jack. The deflection of the specimen is measured using displacement transducers (Linear variable differential transformer, LVDT), as shown in Figure 5, to provide complete information about

Figure 5: LVTD on a concrete slab.

Figure 6: Data logger TDS 530.

deflection in the free end of the beam (1,000 mm from the column flange). All the instruments will be mounted on the specimen when the test specimen is assembled. LVDT are all linked to the data logger TDS-530. Figure 6 shows the data logger TDS-530, which records all data concurrently throughout the test time. Repeated load for each 5 kN was applied to the cantilever at 1,000 mm from the column flange. It easy to get the moment by multiplying the load by the lever arm from the load center to the column flange. The beam rotation magnitude increases according to the distance from the column flange.

Figure 7 shows the testing rig details for composite joint. Each specimen will be carefully examined after the test, including disassembling the joint and removing the bolts. Furthermore, the welding failure mechanism will be studied – showing the rig details, including the composite member. Discussions and comparisons will focus on the important beam–column joint features connected to the moment–rotation capacity relationship.

3 Joint detailing

Five experimental models of composite joint were prepared. The five specimens are denoted as CM1, CM2, CM3, CM4, and CM5. The CM2 model represents the control model for composite beam–column joints. The specimen CM1 comprises a reinforced slab ∅ 10@200 mm, a steel HEA 200 column, a steel IPE 160 beam, and a steel end plate. The CM2 specimen is similar to the CM1 specimen elements except that the CM2 specimen includes column web stiffeners. The CM3 has welded angle stiffeners on the top flange of the beam in addition to column stiffeners. Specimen CM4 consists of elements similar to the control model CM2 with the addition of two stiffeners to the beam (welded web stiffener beam and welded inclined stiffener in the bottom flange of the beam). Finally, CM5 consists of a column stiffener and special reinforcement (continuous rebar in the concrete slab) 25 mm in diameter. Figure 8 shows all types of stiffeners used in this study.

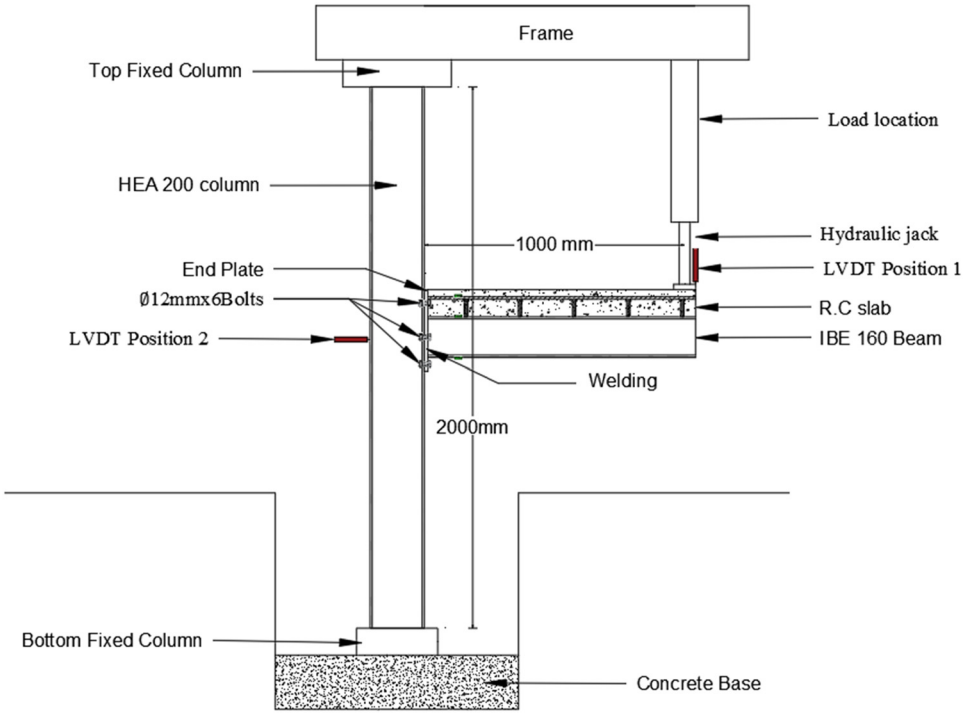

Figure 7: Testing rig details for composite joint.

Figure 8: (a) Column stiffeners of CM2, (b) welded angle stiffener on top flange of beam, (c) welded web stiffener beam and welded inclined stiffener in bottom flange of beam, and (d) special reinforced steel 25 mm diameter.

4 Experimental result and discussion

The results were analyzed by reporting and plotting the considered parameters, comparing the amplitude of each one, and tracing the behavior of the beam with the repeated load using these parameters. The key parameters that affect the behavior of the joint are reported in the experimental program results of the composite beam–column joints. Moment and rotation capacity parameters are selected for studying, comparing, and discussing.

In CM1, no buckling or curvature happens in the steel I beam, and no cracks appear in the concrete slab. The failure mode occurs in column flanges, as shown in Figure 9. The excessive deformation of the column flange and the buckling of the column web were identified as the failure mechanisms in CM1. Since the unstiffened web of column compression resistance was shown to be the weakest component among all the connecting elements, the failure mechanism was anticipated. The disappearing crack in the concrete slab means the reinforced concrete slab is stiff. The column flange was being pushed by the lower part of the beam flange at the maximum rotation of the connection in CM1.

Figure 9: Failure of column flange in CM1.

Additionally, local buckling was found at the column flange due to height tension. However, no failure mode happened on the end plate, and the bolts were still tightened. Figure 10 presents the moment-rotation from experimental results. In CM1, the ultimate moment was 40 kN m in cycle 8 of repeated load with rotations of 66.75×10^{-3} rad for the free end of the composite beam.

The CM2 disassembly was inspected carefully after testing, and the failure modes were observed in specimens due to welding failure between the beam and end plate, as shown in Figure 11. There was no failure mode on the end plate and bolts. No buckling was found in the steel I beam and steel H column. Figure 12 shows that the concrete slab was exposed to a crack in the top surface with 38 kN m in cycle 8. The column web stiffeners convert the failure from column buckling to welded failure in CM2. Transverse stiffeners that were welded to the column web at the level of the top and bottom beam flanges confirmed the column specimens from CM2 to CM5.

The CM1 reached cycle 8, the CM2 achieved cycle 9, and the ultimate moment capacity of CM2 was 42 kN m; with maximum moment in CM2, the rotations were 47.27×10^{-3} rad. Cycle 8 of the repeated load was chosen for rotation comparison between all specimens; in cycle 8, the CM2 rotation was 32.15×10^{-3} rad. Column web stiffeners are seen to raise the ultimate moment by minor values, up to a maximum of 5%, and decrease the rotation by a percentage of 51.8% in cycle 8 compared with CM1. Figure 13 shows moment–rotation curve comparison between CM2

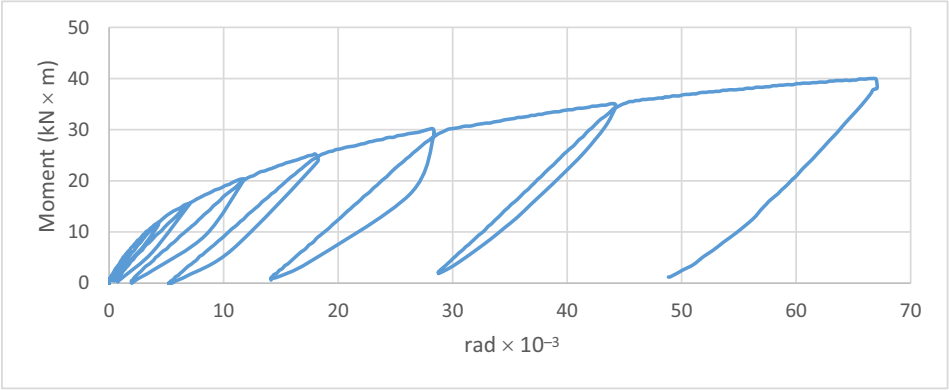

Figure 10: Moment–rotation curve of CM1.

Figure 11: Shape of failure in welding of beam of CM2.

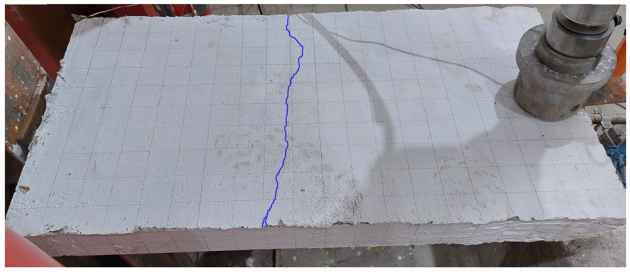

Figure 12: Shape of cracks in reinforcement concrete slab in CM2.

and CM1. Furthermore, the rotational stiffness is increased when the column web is stiffened. The flange of the column bends easily at the point where the column web and flange meet because the column is not stiffened. Nevertheless, many columns were created in compliance with AISC 341 strong-column/weak beam standards [40]. Web column stiffeners reduce deformation in the panel zone joint, but they have no appreciable impact on the final moment. In this study, the CM2 is considered the control specimen for the composite connection joint.

In CM3, it was found that the steel I beam was without buckling, the failure of the specimen was in composite joint connection due to welding failure, as shown in Figure 14, and the reinforced steel in the concrete slab cracked at the top surface when the load reached 37.4 kN as shown in Figure 15.

Figure 16 shows the moment–rotation curve comparison between CM2 and CM3. The ultimate moment in CM3 was 42.3 kN m in cycle 9; the ultimate moment of CM3 is 0.7% more than CM2, which means the ultimate moment is relatively close between CM3 and CM2, the rotation with the ultimate moment was 40.31×10^{-3} rad. However, the rotations with repeated load cycle 40 kN were 24.88×10^{-3} rad; the rotations were reduced to 22.6% compared to CM2. Top angle connections are utilized to convey part of the beam end moment to the column in addition to the vertical reaction, providing lateral support for the compression beam flange. The angle cleats on the top of the beam flange are essential parts of seated connections because they keep the beam stable in a vertical position and prevent it from lateral buckling. Using a welded angle stiffener on the top flange of the beam for CM3 reduced the rotation, and the moment was very close (0.7% increase) in cycle 8 compared with control specimen CM2. Increased CM3 connection performance is achieved by employing a welded angle stiffener on the top flange of the beam. However, the welded angle stiffener on the top flange of the beam strengthens the joint connection, which causes cracks in reinforced concrete.

For the CM4 specimen, Figure 17 shows the failure in welding between the beam and end and Figure 18 shows the buckling failure in specimen CM4 in the bottom flange

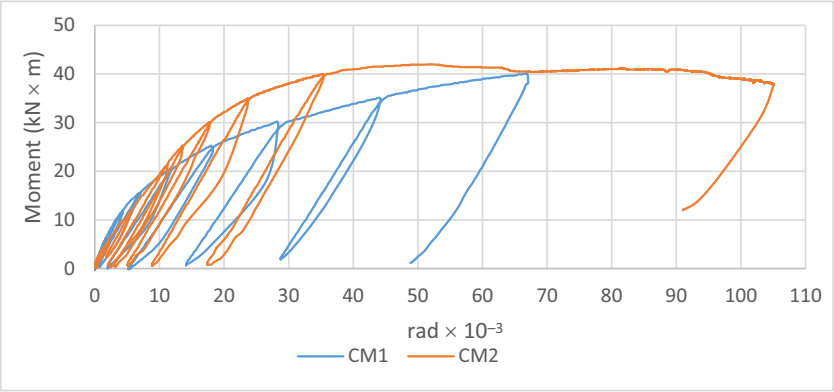

Figure 13: Moment–rotation curve comparison between CM2 and CM1.

Figure 14: Shape of failure in welding of beam of CM3.

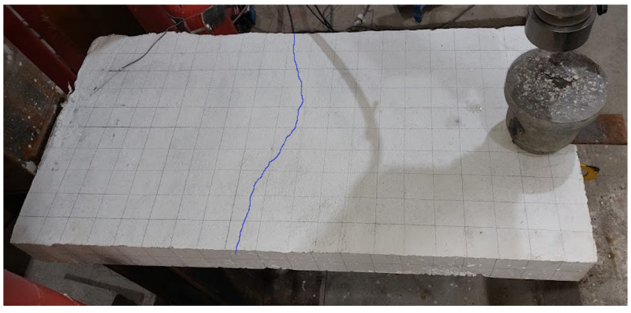

Figure 15: Shape of cracks in reinforcement concrete slab in CM3.

of the beam. Figure 19 shows the crack in the top reinforced concrete slab in cycle 9 with a 42.3 kN applied load. Figure 20 shows moment–rotation curve comparison between CM2 and CM4. The ultimate moment in CM4 was 45 kN m in cycle 9, which is 7.1% more than the ultimate moment in the control model (CM2). The rotations with ultimate moment were 50.81 × 10^{-3} rad. The rotations in cycle 8 for CM4 were 20.95 × 10^{-3} rad, representing a 34.8% decrease in rotation compared with CM2. CM4 specimen had buckling of the bottom beam flange and beam web. The failure was initiated at the bottom beam flange (compression flange) in the form of buckling, followed by buckling of the beam web. The effect of the welded web stiffener beam and welded inclined stiffener in the bottom flange of the beam on CM4 led to increased ultimate moment and decreased rotations. Cracks also appear in reinforced concrete slabs due to enhancing the connection joint's performance and reducing the joint's rotation. When applying jack load on the end of the beam, the load affects the reinforced concrete slab due to buckling failure in the bottom beam flange and beam web in CM4.

The failure in specimens CM5 were in beam (local buckling), as shown in Figure 21; column (local buckling); column rotation, as shown in Figure 22; concrete cracking, as shown in Figure 23; slab crushing, as shown in Figure 24; and failure found in the end plate as shown in Figure 25. The ultimate moment in CM5 was 63.2 kN m in cycle 13; compared with CM2, the ultimate moment of CM5 is 49.4% more than CM2. The rotations in repeated cycle 8 were 14.84 × 10^{-3} rad. Special reinforcement steel with two continues rebars effect on result of CM5 in comparison with control specimen CM2, the rotation in cycle 8 decreased in comparison with control, the rotation decreased 54% in comparison with CM2 and increased the moment capacity.

The previous study characterized an isolated slab with the absence of continuity rebar to the steel H column; in CM5, the study described connecting the column with the slab by continuity of rebar with a 25 mm diameter. The Eurocode 4 for composite steel–concrete joints [41] recommends a "total disconnection" of the slab components close to the column to prevent interaction between the slab and the column. This behavior defies logic and points to the possible activation of resistance mechanisms. On the other

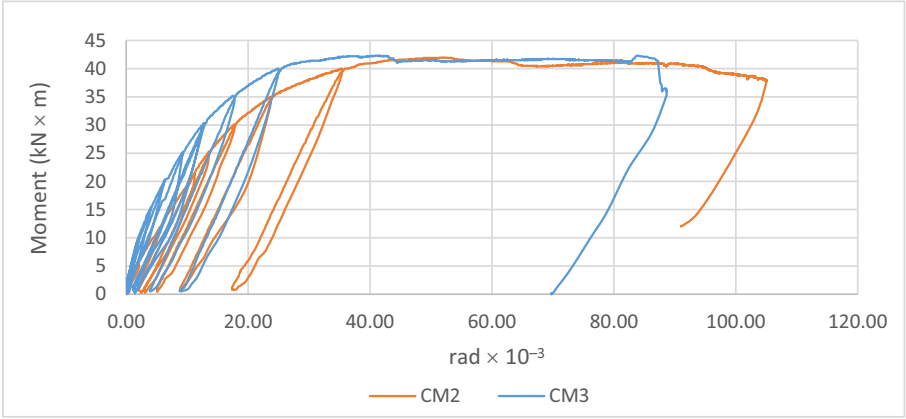

Figure 16: Moment–rotation curve comparison between CM2 and CM3.

Figure 17: Shape of failure in welding of beam of CM4. (a) side view and (b) top view.

Figure 18: Shape of failure in beam of CM4.

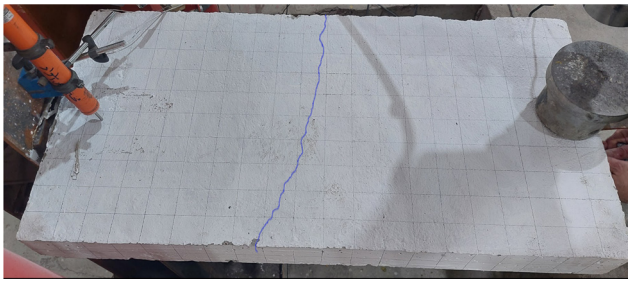

Figure 19: Shape of cracks in reinforcement concrete slab of CM4.

hand, the idea of utilizing the continuity of the longitudinal rebar is examined in this research. It is demonstrated that a connection with an isolated slab and continuous rebars can be used to reduce beam rotation and enhance moment capacity if designed correctly. The structural interaction between the concrete slab and the steel components at the beam-to-column intersection highly affects the composite joints. The experimental results for CM5 summarized in this work demonstrate that the isolation of the slab with continuous rebar is generally linked with significant effects on the structural performance of the joint. as long as there is adequate separation between the slab and the column, even with a small gap. The almost comparable resistance between the continuous rebar and non-continuous rebar from rebars yielding anticipates concrete slab crashing.

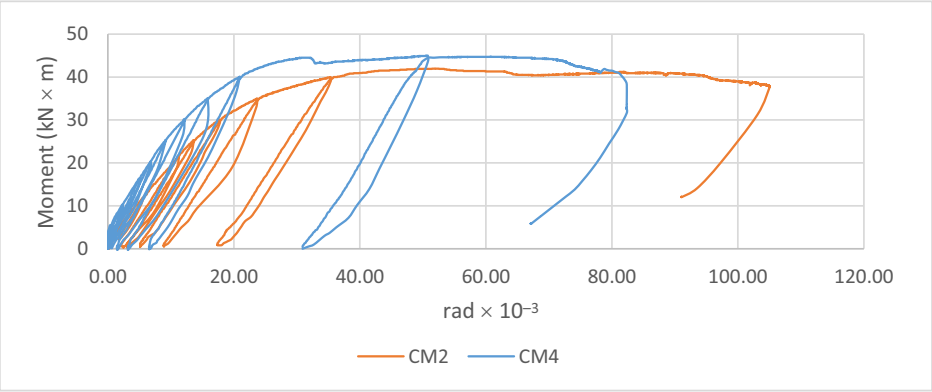

Figure 20: Moment–rotation curve comparison between CM2 and CM4.

Figure 21: Shape of beam failure after testing in CM5. (a) right side and (b) lift side.

Figure 22: Failure of column in CM5.

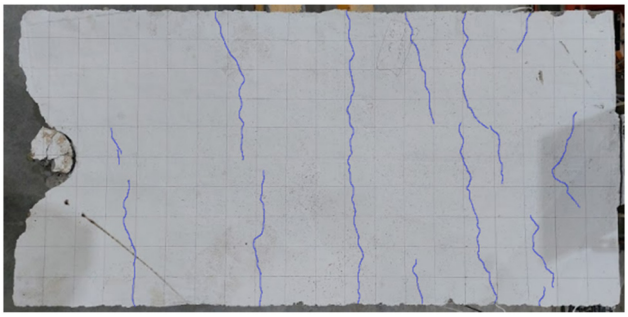

Figure 23: Shape of cracks in reinforcement in CM5.

The total performance of a joint in composite joint systems with an isolated slab and continuous longitudinal rebar has proven to guarantee an increase in bending resistance moment under vertical loads. According to the design guidelines now in use for steel–concrete composite joints, the current results are comparable to isolated slab composite connections without continuous rebars. The CM5 experimental work has enabled the efficient consideration of the contribution of steel members and continuous rebar in concrete slabs. This has facilitated the development of typical mechanisms involving the slab for the complex performance of composite frames under repeated load. Figure 26 shows moment–rotation curve comparison between CM2 and CM5. Figure 27 shows the maximum moment applied for specimens, and Figure 28 shows the rotation of specimens with a 40 kN m applied moment.

Figure 24: Shape of slab crashing in CM5.

Figure 25: Shape of end plate welding with beam after test in CM5.

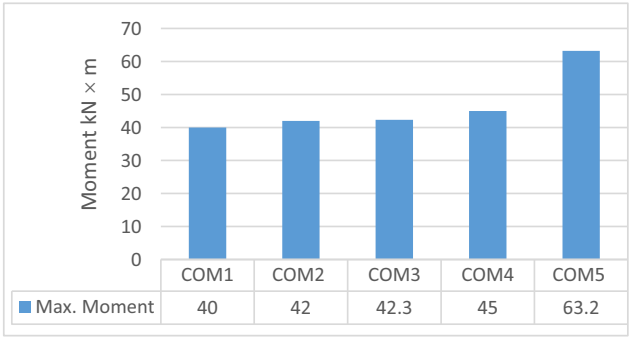

Figure 27: Maximum moment applied for specimens.

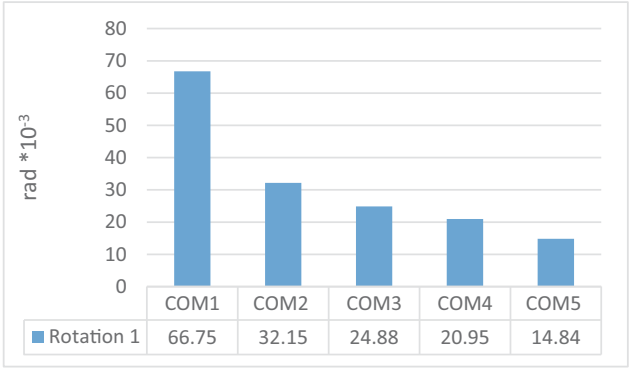

Figure 28: Rotation of specimens with 40 kN m applied moment.

5 FEA

An analysis of FEs was employed to simulate the joint model. Verification is carried out to ensure that the models of CM2 and CM5 described in the experimental test are

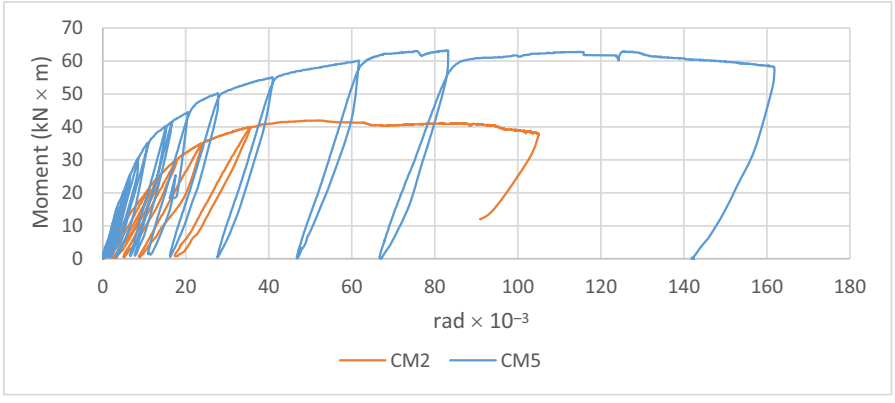

Figure 26: Moment–rotation curve comparison between CM2 and CM5.

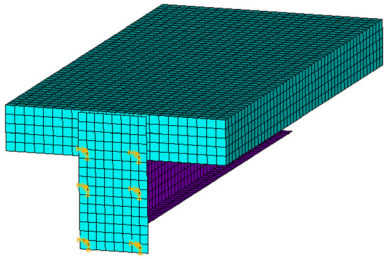

Figure 29: Boundary conditions for the FE model.

valid and accurate. The capability of constitutive models to simulate deflection and stress are all compared. The current study used the FE method in the linear and nonlinear analysis of composite beams. For this presentation, the ANSYS 2022 R1 program was used. The concrete part was represented using a three-dimensional brick element (Solid65) with eight nodes and three degrees of freedom for each node.

In comparison, a two-dimensional shell element (Shell181) with four nodes and six degrees of freedom for each node was used to represent the steel part of the end plate and beam. The reinforcement steel is defined using a one-dimensional element (Link 180) with two nodes and three degrees of freedom for each node. The boundary conditions are applied to the six nodes at the end plates, as shown in Figure 29.

The goal of the contact mechanical interactions was to reproduce every potential contact at the interfaces between the steel and concrete or steel and steel. The connection between the concrete slab and the steel beam is taken to be fully rigid. All of the steel and concrete components were taken into consideration for the experimental mechanical properties, with the steel modulus of elasticity (Es) as 200,000 MPa and the concrete modulus of elasticity (Ec) as 23,025 MPa, Ultimate compressive strength of concrete $f\bar{c}$ = 24.86 MPa, yield strength of steel beam Fy_s = 318.9 MPa, yield strength of the special longitudinal reinforcing steel Fy_r = 482.5 MPa, and yield strength of end plate Fy_e 363.7 MPa. The CM2 and CM5 specimens have a 20 mm gap between the slab and column in FE models to represent the experimental state and ensure no connection between the column and concrete slab for both specimens. The deflection computed by ANSYS compared with those obtained experimentally.

6 FE results

The deflection of the CM2 and CM5 was determined by the FE method using ANSYS software, as shown in Figures 30 and 31, respectively. The maximum deflection appears at the end of the beam for both specimens. Figures 32 and 33 show the experimental and ANSYS load deflection curve

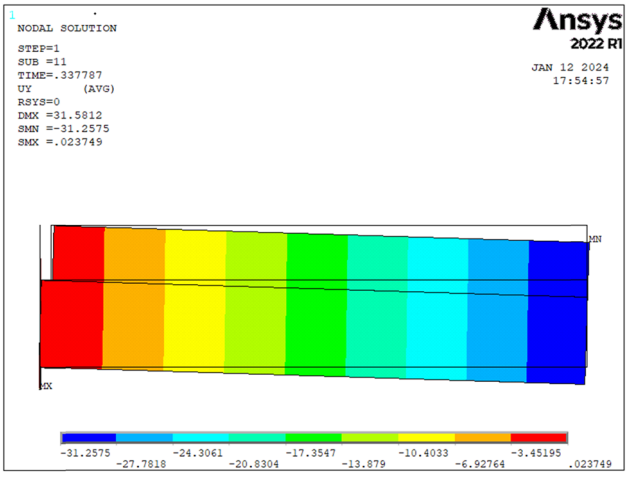

Figure 30: Deflection (mm) of CM2 model predicated by ANSYS.

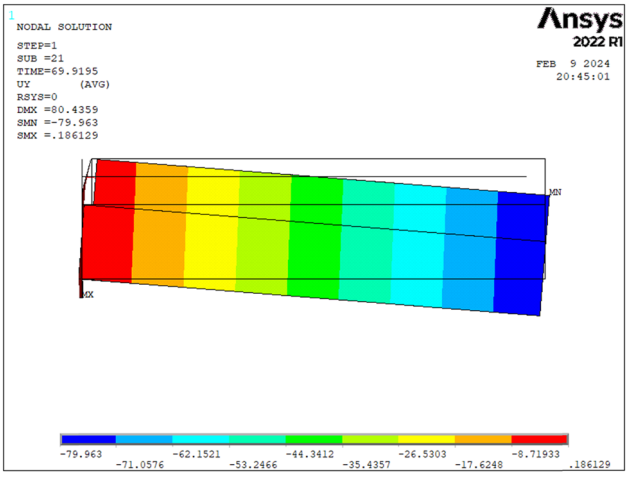

Figure 31: Deflection (mm) of CM5 model predicated by ANSYS.

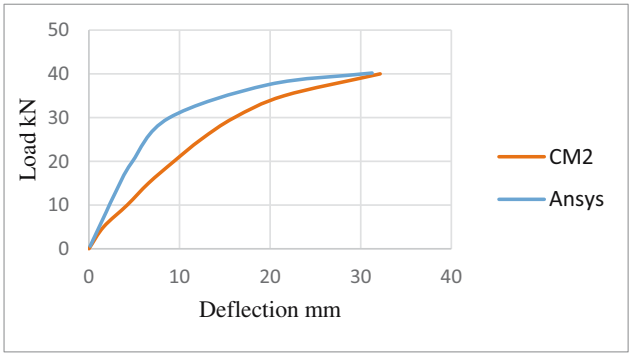

Figure 32: Experimental and ANSYS load deflection curves of CM2.

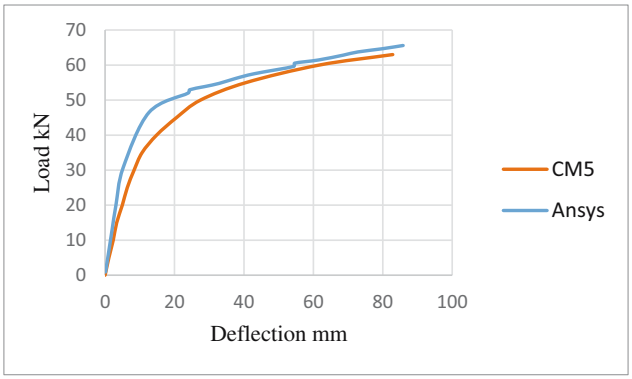

Figure 33: Experimental and ANSYS load deflection curves of CM5.

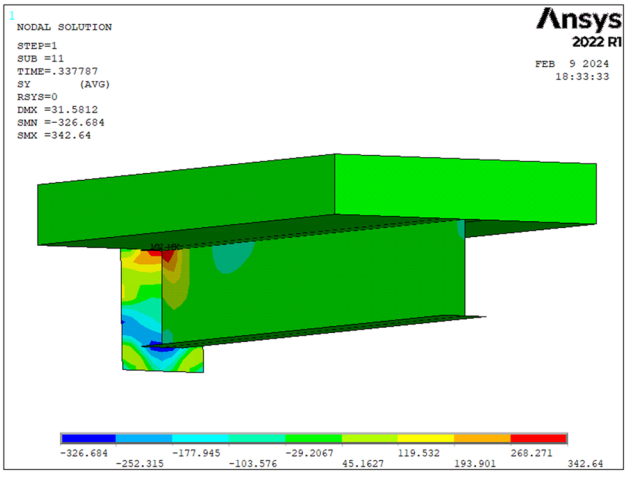

Figure 34: Stress (MPa) of 3D CM2 model predicated by ANSYS.

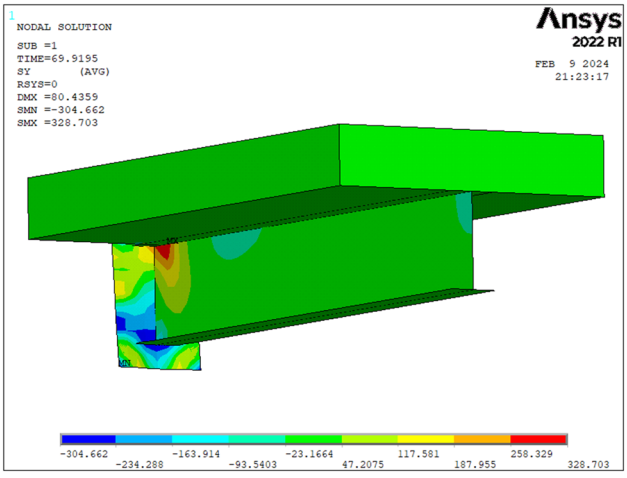

Figure 35: Stress (MPa) of 3D CM5 model predicated by ANSYS.

for CM2 and CM5. The load–deflection curves are in similar behaviors, but the results gained by the ANSYS are stiffer than the experimental result, which is to be expected due to the reasons that the FE models do not take into consideration the microcracks, which could be produced by drying shrinkage or handling that diminish the experimental specimen stiffness. In the FE computations, a complete bond between the steel I beam and concrete slab, as well as steel reinforcement, is assumed. However, there is some slip for the experimental specimen. The action of the composite between the steel beam, concrete, and steel reinforcement decreased as bond-slip occurs. As a result, the experimental stiffness results are expected to be lower than that of the FE models, which, in general, imposes additional behavioral constraints [42]. Other construction flaws also could reduce the rigidity of the actual composite structure elements in experimental works. Full-scale experimental configurations generally agree fairly well with the present FE model due to the presented modelling approach. Most crucially, the concrete slab with continuous rebar and steel members' contributions can be effectively considered, enabling the development of typical mechanisms involving the slab for the complex performance of composite frames under repeated load. Figures 34 and 35 show the stresses for CM2 and CM5, respectively, the stress changes from tension on top of the end plate to compression on the bottom. The maximum tension stress near the top beam flange of the steel I beam is approximately 342 MPa for CM2 and 328 MPa for CM5, and the maximum compression stress near the bottom beam flange of the steel I beam is approximately 326 MPa for CM2 and 304 MPa for CM5. However, the position near the steel I beam mid separates the regions where tension and compression stresses appear. The experimental stress of the end plate was 363 MPa, which is more than the stress found in the FE method. The tension stress can be observed on the top I beam flange near the connection joint, and the compression stress in the bottom I beam flange near the connection joint.

The two scenarios of I beam yield strength considered for the specimens CM2 and CM5, in addition to the original ANSYS scenario of yield strength obtained from experimental work with 318.9 MPa, Figures 36 and 37 show load–deflection curve with various values of yield strength predicated by ANSYS for CM2 model and CM5 model, respectively. The first scenario was increasing the I beam yield strength to 370 MPa. When the beam has a higher yield strength, it becomes stiffer and more rigid and can endure larger stresses before undergoing plastic deformation. Consequently, by reducing the deflection with the same applied load, the load–deflection curve could has a steeper slope. The effect of the second scenario, which decreased the yield strength to 270 MPa, was in contrary

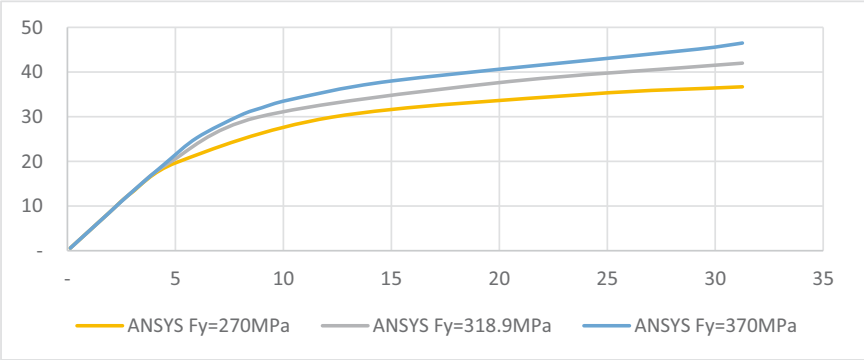

Figure 36: Load deflection curve with various yield strength values predicated by ANSYS for CM2 model.

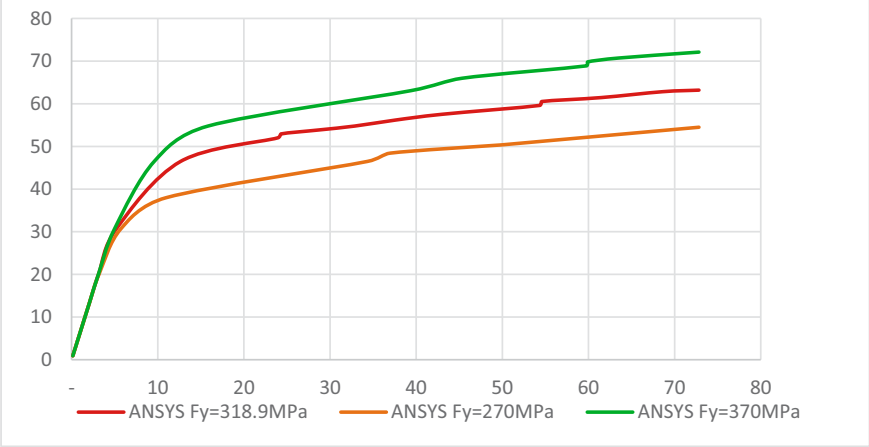

Figure 37: Load deflection curve with various yield strength values predicated by ANSYS for CM5 model.

to the first scenario. In the CM2 model, the maximum loads for yield strengths 270, 318.9, and 370 MPa with the same deflection were 42 kN, 36.7 kN, and 46.5 kN, respectively. The load for yield strength 270 MPa decreased by 13%, and the load for yield strength 370 MPa increased by 11% in comparison with yield strength 318.9 MPa. In the CM5 model, the maximum loads for yield strength 270, 318.9, and 370 MPa with the same deflection were 63.2 kN, 54.5 kN, and 72.1 kN, respectively. The load for yield strength 270 MPa decreased by 14%, and the load for yield strength 370 MPa increased by 14% compared with yield strength 318.9 MPa.

For the CM2 and CM5 models, the thesis presents the parametric study, including the effect of the web on the load–deflection curve. Three web thickness variables are considered (7, 9, and 11 mm) and compared with the thickness of the IPE 160 beam. Figures 38 and 39 show the load–deflection curve with various values of beam web thickness predicated by ANSYS for the CM2 model and CM5 model, respectively.

In the CM2 model, the various values of beam web thickness predicated by ANSYS compared with the web thickness of IPE beam, the load increases with the same deflection to 1.2, 2.1, and 3.3% when using web thickness 7, 9, and 11 mm, respectively. The same procedure was used for CM5 to compare the web thickness of the IPE beam with various values of beam web thickness predicated by ANSYS. The load increased to 0.7, 1.5, and 2.7% when using web thicknesses 7, 9, and 11 mm, respectively. The results show that the Effect of increased web thickness on load and deflection is too small due to the web of the beam being responsible for the shear stress first and foremost.

Another parametric study presents the effect of flange beam thickness on the load–deflection curve. Three variables of flange thickness (9.4, 11.4, and 13.4 mm) were considered and compared with the IPE beam. The load–deflection curve predicated by ANSYS for CM2 and CM5 models with various values of beam flange thickness, respectively, are presented in Figures 40 and 41. The CM2

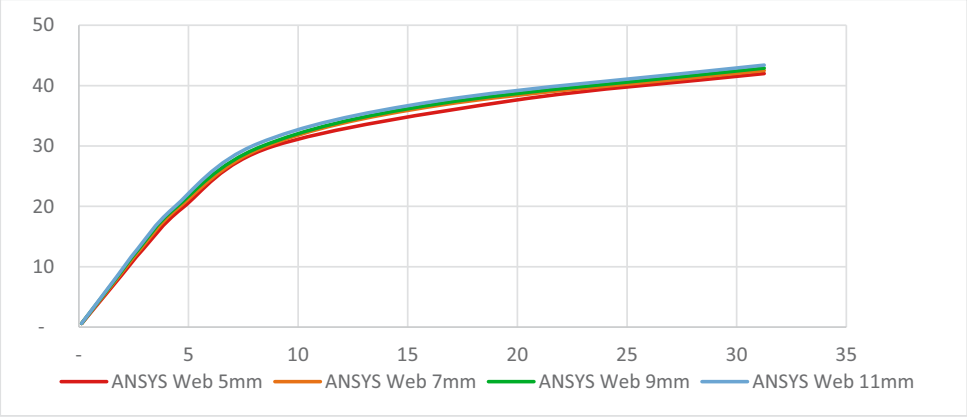

Figure 38: Load deflection curve with various values of beam web thickness predicated by ANSYS for CM2 model.

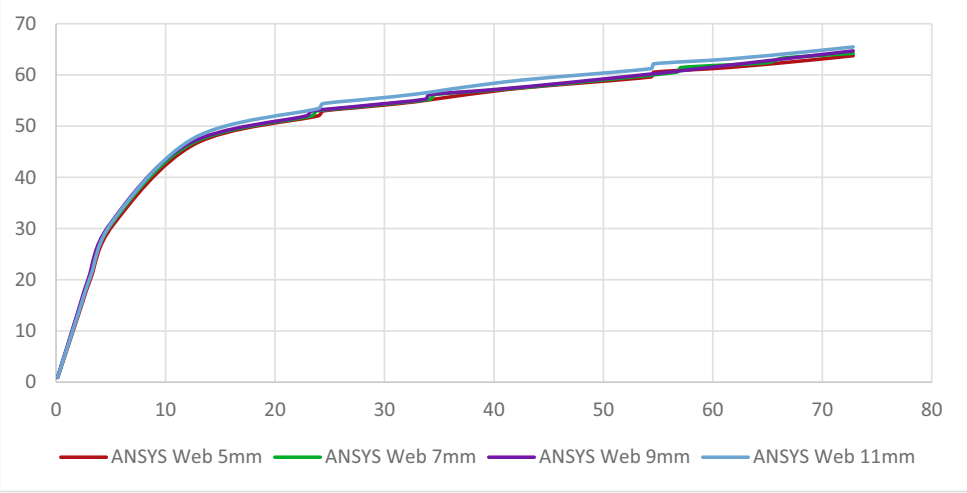

Figure 39: Load deflection curve with various values of beam web thickness predicated by ANSYS for CM5 model.

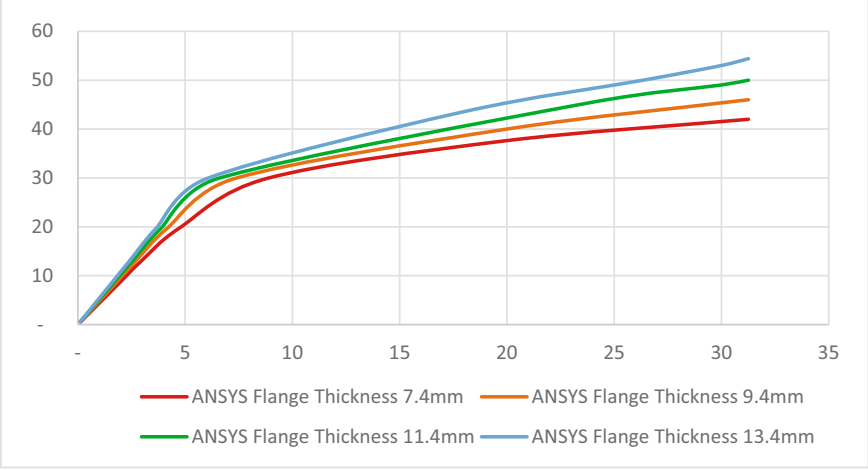

Figure 40: Load deflection curve with various values of beam flange thickness predicated by ANSYS for CM2 model.

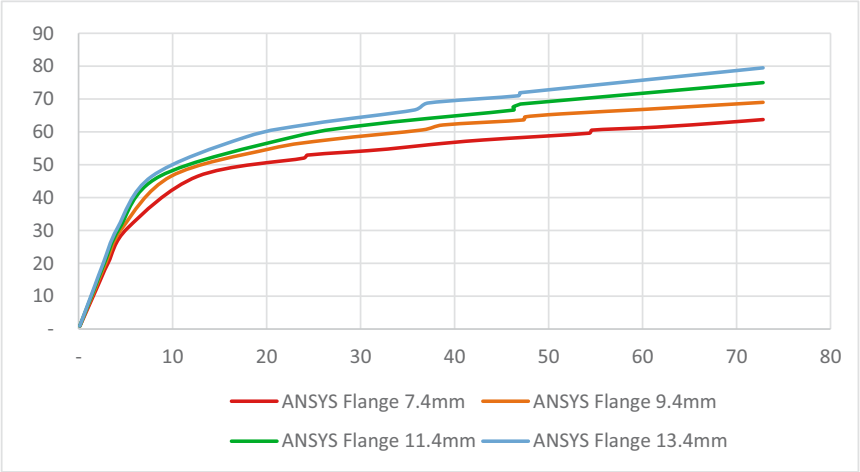

Figure 41: Load deflection curve the various values of beam flange thickness predicated by ANSYS for CM5 model.

load increased by 9.5, 19, and 29.5% compared with IPE 160 flange thickness when using various beams flange thickness predicated by ANSYS 9.4, 11.4, and 13.4 mm, respectively. The CM5 load increased by 8.2, 17.6, and 24.7% compared with IPE 160 flange thickness when using flange thicknesses of 9.4, 11.4, and 13.4 mm, respectively. The curves show an increase in load resistance with a rise in beam flange thickness; this is because the majority of the moment applied to the beam is carried by the flange of the beam. The flanges resist most of the moment because they are geometrically farther from the neutral axis, which results in a longer moment arm.

7 Conclusion

The following are the principal findings of the study:

- In the CM2 specimen, rotation is reduced by 51.8% in cycle 8 when column web stiffeners are utilized. It enhances the ultimate moment by very small amounts, within 5%, even though it has no discernible impact on the ultimate moment. In addition, the rotational stiffness of the connection is enhanced when the column web stiffens.
- Following the formation of the first crack, the rotational stiffness of the specimens did not significantly diminish, meaning that the connection remained firm. This occurred due to the concrete slab's continued stiffness as the cracks had not broken through it. As a result, there was little decrease in the connection rotational stiffness.
- The ultimate moment in CM3 is 0.7% greater than CM2, meaning these two models have relatively close ultimate moments. When comparing CM3 to CM2, the rotations decrease to 22.6% in CM3. The ultimate moment in CM4 was 7.1% more than in the control model (CM2). The rotations for CM4 indicated a drop in rotation of about 34.8%. The ultimate moment for CM5 in cycle 13 was 63.2 kN m. This means that the ultimate moment for CM5 is 49.4% more than CM2. The results of CM5 showed a decrease in rotation by 54% in cycle 8 compared to control specimen CM2. This was due to the special reinforcement steel effect. Through the study, it can be concluded that the specially reinforced rebar with 25 mm in diameter has significantly affected the model moment capacity and rotation. Including the contribution of steel members and continuous rebar in concrete slabs enables the development of typical mechanisms involving the slab to perform composite frames subjected to repeated load.
- In CM1, the failure mode that occurs in column flanges was determined. For CM2, CM3, and CM4, the failure modes were observed in specimens due to welding failure between the end plate and beam. The failure mode for CM4 was in welding between the beam and end plate, as well as the buckling failure in the bottom flange of the beam. The failure modes in specimen CM5 were in the beam (local buckling), column (local buckling), column rotation, concrete cracking, slab crushing, and failure found in the end plate.
- The load–deflection curves for CM2 and CM5 in the FE models have behaviors similar to the experimental load–deflection curve. Still, the results gained by the ANSYS are stiffer than the experimental result, which is to be expected because the FE models do not consider the microcracks.
- The stress changes from tension on top of the end plate and beam flange to compression on the bottom and beam

flange. The maximum tension stress is near the top beam flange, and the maximum comparison stress is near the bottom beam flange. For CM2 and CM5, the maximum tension stress is approximately 342 and 328 MPa, respectively, near the top beam flange of the steel I beam. The maximum compression stress for the steel I beam is approximately 326 MPa for CM2 and 304 MPa for CM5 when measured close to the bottom beam flange. Nonetheless, the location close to the steel I beam's midpoint divides the regions where compression and tension stresses are present. The experimental stress measured on the end plate was 363 MPa, higher than the stress determined using the FE method. The exposed welding failure in the composite beam can be explained by the stress concentration in the top and bottom flanges.

- According to the parametric I beam yield strength study based on ANSYS for CM2 and CM5, higher yield strength is more rigid and stiffer. It can withstand higher loads before experiencing plastic deformation. Consequently, the deflection will be reduced with the same applied load. When using 370 MPa yield strength, the load increased to 11 and 14% for CM2 and CM5, respectively, and when changing the yield strength to 270 MPa, the load decreased to 13 and 14% for CM2 and CM5, respectively, compared to original yield strength of beam (318.9 MPa).
- The parametric analysis determines that compared to the thickness of the IPE 160 beam for CM2, the influence of web thickness (7, 9, and 11 mm) predicted by ANSYS on the load was 1.2, 2.1, and 3.3%, respectively. According to ANSYS, the impact of different web thicknesses (7, 9, and 11 mm) on the load was 0.7, 1.5, and 2.7% for CM5. The results show that increasing the web thickness has too little impact on load and deflection since the beam's web is primarily responsible for shear stress.
- The load increases by 9.5, 19, and 29.5% for the CM2 when different beam flange thicknesses are used, as determined by ANSYS, which are 9.4, 11.4, and 13.4 mm, respectively, in comparison to IPE 160 flange thickness. The load increases by 8.2, 17.6, and 24.7% for the CM5 when flange thicknesses of 9.4, 11.4, and 13.4 mm are used, respectively, compared to IPE 160 flange thickness. The parametric results indicate that load resistance increases as beam flange thickness increases. This is because most of the moment applied to the beam is carried by the beam's flange. The flanges resist most of the moment because they are geometrically farther from the neutral axis, which results in a longer moment arm.

Acknowledgements: The authors are grateful for the reviewer's valuable comments that improved the manuscript.

Funding information: Authors state no funding involved.

Author contributions: All authors have accepted responsibility for the entire content of this manuscript and consented to its submission to the journal, reviewed all the results and approved the final version of the manuscript. SYKA-D and BJMA-S devised the project: the main conceptual ideas, and proof outline. LKA worked out almost all of the technical details, and performed the numerical calculations for the suggested experiment with help from SYKA-D. BJMA-S verified the experimental and numerical results. LKA prepared the manuscript with contributions from all co-authors. All authors discussed the results and contributed to the final manuscript.

Conflict of interest: Authors state no conflict of interest.

Data availability statement: The datasets generated and analyzed during the current study are available from the corresponding author on reasonable request.

References

[1] Handhal MM, Abdulghani AW, Al-Haydary MM. Structural behavior of steel reinforced concrete joint under flexural loads. Civ Eng J. 2023;9(3).

[2] BEng SH, Park S. EN 1994-Eurocode 4: Design of composite steel and concrete structures. Berkshire, UK: Report of e Steel Construction Institute; 1994.

[3] Da Silva LS, Simoes RD, Cruz PJ. Experimental behaviour of end-plate beam-to-column composite joints under monotonical loading. Eng Struct. 2001;23(11):1383–409.

[4] Couchman GH, Way AG. Joints in steel construction: Composite connections. Steel Construction Institute; 1998.

[5] Aminuddin K, Saggaff A, Tahir MM. Experimental behaviour of beam-column connection using cold-formed steel sections with rectangular gusset-plate. AIP Conference Proceedings. AIP Publishing LLC; 2017. p. 020006.

[6] Xiao Y, Choo B, Nethercot D. Composite connections in steel and concrete. I. Experimental behaviour of composite beam–Column connections. Journal of Constructional Steel Research. 1994;31(1):3–30.

[7] Anderson D, Najafi A. Performance of composite connections: major axis end plate joints. J Constr Steel Res. 1994;31(1):31–57.

[8] Liew JR, Teo T, Shanmugam N, Yu C. Testing of steel–concrete composite connections and appraisal of results. J Constr Steel Res. 2000;56(2):117–50.

[9] Kuhlmann U, Rolle L, Jaspart J, Demonceau J, Vassart O, Weynand K, et al. Robust structures by joint ductility, Final Report. Germany: Science Research Development, European Commission; 2009.
[10] Malaska M. Behaviour of a semi-continuous beam-column connection for composite slim floors. Helsinki, Finland: Helsinki University of Technology; 2000.
[11] Demonceau J-F, Jaspart J-P. Experimental test simulating a column loss in a composite frame. Adv Steel Constr. 2010;6(3):891–913.
[12] Guo L, Gao S, Wang Y, Zhang S. Tests of rigid composite joints subjected to bending moment combined with tension. J Constr Steel Res. 2014;95:44–55.
[13] Sun F, Sun M, Li G, Xiao Y, Wei M, Liu L. Experimental study on seismic behavior of high-strength steel beam-to-column end-plate connections. J Build Struct. 2014;35(4):116–24.
[14] Muresan IC. Research on analysis and design philosophy of the connections in steel structures. Cluj-Napoca, Romania; 2015.
[15] Wang J, Wang J, Wang H, eds. Seismic behavior of blind bolted CFST frames with semi-rigid connections. Structures. Romania: Elsevier; 2017.
[16] Song T-Y, Tao Z, Razzazzadeh A, Han L-H, Zhou K. Fire performance of blind bolted composite beam to column joints. J Constr Steel Res. 2017;132:29–42.
[17] Zandonini R, Baldassino N, Freddi F, Roverso G. Steel-concrete frames under the column loss scenario: An experimental study. J Constr Steel Res. 2019;162:105527.
[18] Firdaus M, Saggaff A, Tahir MM, Ngian SP, Aminuddin K, Saloma S. Experimental study of composite connections for cold-formed steel using isolated joint test. Journal of Physics: Conference Series. IOP Publishing; 2019.
[19] Vishawadeep SG. FEM analysis of steel beam column joint by using cantilever weight and acceleration. J Ceram Concr Sci. 2019;3(3):16–24.
[20] Chen K, Yang B, Zhang Y, Tan KH. Experimental tests on composite beam-column joint with WUF-B connection subjected to impact loads. Int J Impact Eng. 2023;174:104506.
[21] Skarmoutsos G, Kuhlmann U. Seismic behaviour of dissipative beam-to-column steel and steel-concrete composite joints. ce/papers. 2023;6(3–4):2232–7.
[22] Salah MS, Muteb HH, Hamad MA. The structural behavior of composite cold-formed steel beam-to-column joints with different connection shapes. J Build Pathol Rehabilitation. 2023;8(1):50.
[23] Loh H, Uy B, Bradford M. The effects of partial shear connection in composite flush end plate joints Part I – experimental study. J Constr Steel Res. 2006;62(4):378–90.
[24] Fu F, Lam D, Ye J. Modelling semi-rigid composite joints with precast hollowcore slabs in hogging moment region. J Constr Steel Res. 2008;64(12):1408–19.
[25] Wang J-F, Li G-Q. A practical design method for semi-rigid composite frames under vertical loads. J Constr Steel Res. 2008;64(2):176–89.
[26] Fu F. 3-D nonlinear dynamic progressive collapse analysis of multi-storey steel composite frame buildings – Parametric study. Eng Struct. 2010;32(12):3974–80.
[27] Piluso V, Rizzano G, Tolone I. An advanced mechanical model for composite connections under hogging/sagging moments. J Constr Steel Res. 2012;72:35–50.
[28] Askar M, Abduka K, Askar L. Seismic vulnerability assessment of reinforced concrete structures in Kurdistan Region-Iraq. J Duhok Univ. 2020;23(2):116–30.
[29] Khandelwal K, El-Tawil S. Collapse behavior of steel special moment resisting frame connections. J Struct Eng. 2007;133(5):646–55.
[30] Li H, El-Tawil S. Three-dimensional effects and collapse resistance mechanisms in steel frame buildings. J Struct Eng. 2014;140(8):A4014017.
[31] Kim S, Lee C-H, Lee K. Effects of floor slab on progressive collapse resistance of steel moment frames. J Constr Steel Res. 2015;110:182–90.
[32] Askar LK, Albarwary IHM, Askar MK. Use of expanded polystyrene (EPS) beads in silica-fume concrete. J Duhok Univ. 2019;22(1):30–8.
[33] Song Y, Uy B, Wang J. Numerical analysis of stainless steel-concrete composite beam-to-column joints with bolted flush endplates. Steel Compos Struct. 2019;33(1):143–62.
[34] Kochem RFF, Nardin SD. Numerical model of beam-to-column composite connection between slim floor system and composite column. Rev IBRACON de Estrut e Materiais. 2020;13:348–79.
[35] Mou B, Zhao F, Wang F, Pan W. Effect of reinforced concrete slab on the flexural behavior of composite beam to column joints: Parameter study and evaluation formulae. J Constr Steel Res. 2021;176:106425.
[36] Mou B, Yan X, Yu Y, Wang Z. Composite CFST column to H-shaped steel beam joint: Experimental and numerical investigation. Eng Struct. 2024;299:117083.
[37] Fasan M, Bedon C, Amadio C, Pecce MR. Non-linear component-based modelling strategy for beam-to-column steel-concrete composite joints under seismic loads. J Constr Steel Res. 2024;212:108314.
[38] Balamuralikrishnan R, Al-Mawaali A, Al-Yaarubi M, Al-Mukhaini B, Kaleem A. Seismic upgradation of RC beams strengthened with externally bonded spent catalyst based ferrocement laminates. HighTech Innov J. 2023;4(1):189–209.
[39] Rajić A, Lukačević I, Skejić D, Ungureanu V. Cold-formed steel-concrete composite beams with back-to-back channel sections in bending. Civ Eng J. 2023;9(10):2345–69.
[40] Malley J, Arber L, eds. An overview of the changes to AISC 341 – Seismic provisions for structural steel buildings. Structures Congress. Reston, VA: American Society of Civil Engineers; 2018.
[41] Standardization ECf. Eurocode 4: Design of composite steel and concrete structures – Part 1.1: General rules and rules for buildings. UK: British Standards Institute; 2004.
[42] Plans A, Grau D, Soltanalipour M, Ferrer-Ballester M, Marimon F, Andreu A. Three-dimensional finite element modeling for bending and pull-out tests of composite slabs. Eng Struct. 2023;295:116785.